From lakes to ratios : 14C measurement process of the Finnish tree-ring research consortium

Uusitalo, Joonas

Elsevier B.V.
2022-05-15

Uusitalo, J, Arppe, L, Helama, S, Mizohata, K, Mielikäinen, K, Mäkinen, H, Nöjd, P, Timonen, M & Oinonen, M 2022, 'From lakes to ratios : 14C measurement process of the Finnish tree-ring research consortium', Nuclear Instruments and Methods in Physics Research, Section B: Beam Interactions with Materials and Atoms, vol. 519, pp. 37-45. https://doi.org/10.1016/j.nimb.2022.03.0

http://hdl.handle.net/10138/575395
10.1016/j.nimb.2022.03.013

From lakes to ratios: ^{14}C measurement process of the Finnish tree-ring research consortium

Joonas Uusitalo[a,b], Laura Arppe[a], Samuli Helama[c], Kenichiro Mizohata[a,b], Kari Mielikäinen[d], Harri Mäkinen[d], Pekka Nöjd[d], Mauri Timonen[c] & Markku Oinonen[a]

[a] Finnish Museum of Natural History, P.O. Box 64, 00014 University of Helsinki, Finland

[b] Department of Physics, P.O. Box 64, 00014 University of Helsinki, Finland

[c] Natural Resources Institute Finland, Ounasjoentie 6, 96200 Rovaniemi, Finland

[d] Natural Resources Institute Finland, Tietotie 2, 02150 Espoo, Finland

Corresponding authors:

Joonas Uusitalo, Gustaf Hällströmin katu 2, 00014, Helsinki, Finland, joonas.uusitalo@helsinki.fi

Markku Oinonen, Gustaf Hällströmin katu 2, 00014, Helsinki, Finland, markku.j.oinonen@helsinki.fi

Abstract

Annual and sub-annual tree-ring ^{14}C measurements allow the study of past natural phenomena such as rapid ^{14}C increases and solar behavior. In addition, they provide precise calibration data sets that help in improving the dating accuracy of past natural and cultural events. However, for the data to be comparable, it is important that laboratories describe the whole process from sample retrieval to eventual results. In this paper, we describe the full ^{14}C measurement procedure adopted in the Finnish tree-ring consortium, including sample collection and preparation, dendrochronology, chemical pretreatment, combustion and graphitization, Accelerator Mass Spectrometry (AMS) measurements and data processing. In addition, we report the ^{14}C background components for our traditional Closed-Tube Combustion (CTC) and Elemental Analyzer (EA) based processes, both yielding to high-quality data. Furthermore, we study the mass-dependence effects of tree-ring measurements and find them to be practically insignificant for ages up to several millennia but growing in significance when approaching the ^{14}C limit.

Keywords

^{14}C analytics, AMS, blank corrections, dendrochronology, sample pretreatment

1 Introduction

The finding of the rapid ^{14}C excursion in tree rings around AD 774 [1] started the trend towards increasing annual ^{14}C measurements. After the initial discovery, it has become evident that the historical atmospheric ^{14}C concentrations have occasionally changed more dramatically than what has been previously thought based on lower resolution measurements. So far, similar rapid events have been suggested around years AD 993 [2], 660 BC [3–5], 5480 BC [6], 800 BC [7] and AD 1055 [8]. In addition to providing important insights into the causes of such events, rapid ^{14}C spikes can work as pointer years when anchoring and identifying geological phenomena such as volcanic eruptions and historical events [9–12]. Furthermore, annually resolved ^{14}C measurements have recently shed light on the timing of the historically meaningful

Minoan eruption of Thera/Santorini [13–16]. In addition, these measurements have further illuminated the often subtle but quantifiable ^{14}C offsets between high-resolution measurements from different geographical locations, growing conditions, laboratories etc., already discussed in Stuiver and Braziunas (1998) [17] and more recently demonstrated by Uusitalo et al. (2018) [18] and Büntgen et al. (2018) [19] with the AD 774 event and for Arctic regions, in particular.

The importance of annual and even sub-annual [18] measurements will further grow as they allow for more precise age calibrations. It is foreseeable that eventually the whole Holocene will be covered by an annually resolved ^{14}C calibration curve, constructed through measurements from multiple laboratories and different isoscapes i.e. geographies, tree-species, climate conditions etc. As the database grows, it might even become feasible to take advantage of the fine structure, e.g. solar cycle, and local and seasonal conditions to radically improve the dating accuracy [16]. However, the older the sample and the smaller the mass of measured carbon, the larger is the potentially biasing role of ^{14}C background induced by the measurement process. Particularly, understanding of the mass-dependent effects have become a crucial element of ^{14}C analytics [20–22]. As wood grows slowly in the Arctic conditions, the availability of wood material from tree rings may become limited, these effects thus requiring special attention within the northern latitudes. Therefore, it is important to describe and document the full ^{14}C tree-ring measurement procedure including sample collection, preparation, chemical pretreatment, combustion, graphitization and Accelerator Mass Spectrometry (AMS) measurement and to quantify the amount of process contaminants so that the quality and the possible error sources can be well understood. This paper fulfils this request.

A consortium between University of Helsinki (UH) and Natural Resources Institute Finland (Luke) was established in 2010 to contribute in stable isotopic and radiocarbon measurements on the long Arctic tree-ring chronology of northern Finland and presently involves researchers and facilities from Finnish Museum of Natural History (Luomus) / UH, Accelerator Laboratory / UH and Luke. In this paper we describe the full process of radiocarbon measurements of tree-ring cellulose by the consortium. We report our ^{14}C large-mass blank values from various processes collected during recent years, perform a test measurement set using tree samples close to the ^{14}C background with varying sample masses, study the implications of mass-balance contamination effects, suggest analysis protocol for typical large-mass AMS graphites (>1 mg), and describe a correction protocol for small-sample (<1 mg) analyses. In addition, we discuss the age-dependent effects of the ^{14}C background levels for samples from modern to ca. 50 000 BP ages corresponding to periods of time in which we foresee to contribute to ^{14}C research in the future.

2 Materials and Methods

2.1 Sample retrieval, pretreatment and cross-dating

Tree-ring ^{14}C data can be obtained from different sources of wood materials: living trees, dead trees preserved as subfossils in natural deposits and wooden samples available from historical and archaeological constructions or objects [23,24]. Living trees are the primary source for tree-ring materials over the recent decades and centuries. Tree-ring material of this type are commonly obtained as core samples, at breast height (ca. 1.3 m), using increment borers (Fig. 1a). In Finland, Scots pine (*Pinus sylvestris* L.) trees older than 150 years are not uncommon but in rare cases the length of the tree-ring samples of the species may reach even 500-600 years (e.g. Lindholm (1996) [25]). However, the distribution of old (≥150 years) trees is uneven through the country, the old trees being typically found from northern Finland [26]. Extended chronologies and older sample materials are to be obtained from dead trees. In favourable condition, typically limited to dry forest soils or mountainous terrain, dead and decaying trees may remain subaerially preserved as standing or fallen tree trunks for more than 1000 years [27,28]. Subfossil materials even older

than this may be obtained from depositional settings where the preservation potential of deposited wood is increased by anoxic conditions. Finland is “a land of a thousand lakes” and the possibility of retrieving subfossil trees lying in the lacustrine sediments have been explored for different parts of the country [29–34]. Importantly, the ‘supra-long’ tree-ring chronology of *P. sylvestris* collected from the lake sites in northern Finland covers the past 7.6 thousand years [30,35,36] providing an excellent source for mid and late Holocene ^{14}C records. Beyond the Holocene, rare sample material can be found in interglacial sediment or peat deposits. For instance, an 8 m long and 40 cm thick trunk of *Larix* was found from a depth of 4.5 m within an interglacial sand layer during an excavation of Vuotso canal connecting water reservoirs of Lokka and Porttipahta in northern Finland. It was originally radiocarbon dated as >49200 BP (Su-826) and considered representing Eemian interglacial of 115 – 130 ka [37]. In this work, this particular material, with the sample labelled as 30/KAM/79, was used for ”^{14}C-dead” blank samples.

Regarding the most common sample material at lake sites, the subfossil tree trunks are pulled to the shore and sawn into disks, after which the trunks are returned into the lake sediments (Fig. 1b-c). Similar to such subfossil materials, tree-ring samples (discs) may be cut from historical or archaeological wooden constructions. In the lab, each tree-ring sequence is cross-dated in accordance with the basic principles of dendrochronological techniques and methods [38,39] and using the statistical software tailored for this purposes [40,41]. Cross-dating is carried out relying on the synchrony of the narrow and wide annual rings due to common signal in tree-ring data. To do so, tree-ring widths are measured under light microscope to the nearest one-hundredth of a millimetre. Alternatively, cross-sectional surface areas of the discs can be sanded and scanned for analyses of digital images. Annual ring-boundaries are then marked from the images and the resulting series of ring widths measured with aid of CooRecorder software [42]. According to research targets, cross-dated tree-ring sequences may then be selected for ^{14}C analyses of a certain time interval. Alternatively, the tree-ring sequence may remain undated to calendar years and the resulting ^{14}C data may enter the procedure of wiggle-matching [43–45] to date the series of ^{14}C ages by fitting their pattern against the fluctuations present in the calibration curve. Dissecting the tree-ring samples is done using a sterile surgical blade under the microscope (Fig. 1d). Commonly, the samples are dissected annually where the boundary from one ring to next (i.e. the latewood-earlywood boundary) is used to divide the sample material (Fig. 1e), no cross-contamination being allowed in the process by visual inspection. Samples may alternatively be dissected sub-annually, in which case the earlywood and latewood portions of each annual ring are being separated during the sampling. In this case, the separation of the earlywood and latewood of the same calendar year is judged by the intra-annual cellular characteristics (i.e. the earlywood-latewood boundary) discernible on the cross-sectional surface of the sample, generally following the established criteria [46]. This work results in flakes and slivers of wood being then entered into the 2 ml screwcap microtubes and kept frozen until used for cellulose and isotope processes.

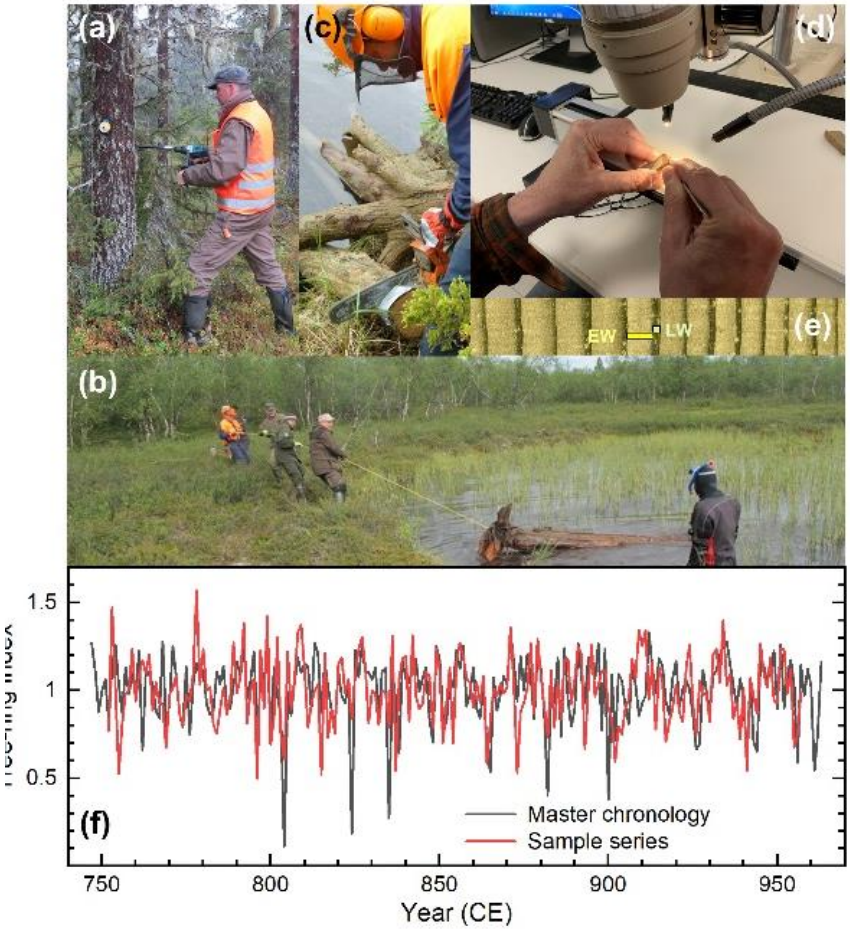

Figure 1. Tree-ring work in the fieldwork and laboratory. (a) Tree-ring samples were extracted from standing trees using 10 mm diameter Haglöf borer (Haglöf Sweden AB, Långsele, Sweden) attached to Makita DHP481RTJ electric drill (Makita Jan-Baptist, Vinkstraat 2, 3070, Belgium) powered by Li-ion Makita BL1850 batteries (Makita Corporation, Anjo, Aichi, Japan), by the aid of an adapter specifically manufactured in a metal workshop to this special purpose. (b) Unearthing a subfossil tree trunk from lacustrine sediment. (c) Sawing a subfossil trunk pulled to the shore. (d) Dissecting tree-ring samples by a surgical blade under the microscope. (e) Scanned image of a tree-ring sequence representing subfossil Scots pine (Pinus sylvertris L.) sample showing the constituents of an annual ring (i.e. tree-ring) depicted as yellow rectangle for earlywood (EW), which in lighter-coloured part of the annual ring, and green rectangle for latewood (LW), which is the darker-coloured part of the ring. (f) Tree-ring cross-dating of a sample series (Uusitalo et al. 2018 [18]) against the existing master chronology [30,35,36]. Photos by Hannu Herva (a, b, e), Mauri Timonen (c), and Samuli Helama (d).

2.2 Sample pretreatment

The tree-ring material is processed into α-cellulose (Fig. 2) due to its long-term stability and consistent isotopic character among the different wood constituents (e.g. Savard et al. (2012) [47]). The setup for the extraction process is based on the MSISS system presented by Wieloch et al. (2011) [48] consisting of a vacuum filtering flask, a pump and four interconnected 40-slot PTFE blocks with internal drainage conduits (Fig. 2), facilitating simultaneous cellulose extraction of 160 whole wood samples contained in filter funnels. The treatment solutions are evacuated between each step using the pump/vacuum filter flask

system. The wood slivers, stored in a freezer (-16 °C) prior to extraction, are placed into custom-made, frit bottomed borosilicate glass funnels attached to the slots of the PTFE block. An individual sample typically weighs 2-50 mg. Samples larger than 50 mg are split into two or more funnels.

The extraction process follows that of the Potsdam Dendro Laboratory described in Wieloch et al. (2011) [48] omitting pre-extraction steps using organic solvents [49]. The procedure takes place in a water bath held at 60 °C having water level slightly higher than the solution where the samples lie. The wood slivers are first treated with a 5% NaOH solution. After two hours, the solution is evacuated and replaced with fresh 5% NaOH and treated for another two hours. The samples are then washed repeatedly with sub-boiling MilliQ® water until the solute is neutral. Next, the samples are subjected to a 37 hour treatment with a 7% $NaClO_2$ solution acidified to pH 4-5 with 100% acetic acid. The initial $NaClO_2$ solution is replaced three times for a total of four consecutive treatments lasting ten, seven, ten and ten hours, respectively. The $NaClO_2$ solution is prepared for each batch right before use. After the last $NaClO_2$ treatment, the water bath is drained, and the samples are washed with sub-boiling MilliQ® water to neutrality, and treated with 17% NaOH for two hours at room temperature. If the samples have not reached a bleached white colour at this stage, they are further treated with an additional 10 hour $NaClO_2$ treatment (at 60 °C), followed by a 2 hour 17% NaOH treatment. To finish the extraction process, the samples are washed with a 1% HCl solution, followed by repeated rinses with sub-boiling MilliQ® water until the solute is neutral. During all treatment steps, special attention is payed to making sure the wood slivers are totally immersed in the treatment solution. To avoid any contamination between successive treatment batches, the borosilicate funnels are cleaned between extractions by combustion at 500 °C for three hours, subsequently soaking them in 5% HCl for 24 hours, repeated MilliQ rinses and a final 24 hour soak in MilliQ® water.

The extracted α-cellulose is transferred from the funnels to 2.0 ml polypropylene microtubes with tweezers, immersed in 1-1.5 ml MilliQ® water and refrigerated for a minimum of 12 hours to facilitate fiber swelling and easier homogenization. Cellulose extracts from large samples split and processed in two or more funnels are combined at this stage. The cellulose is homogenized using an ultrasonic device (Hielscher Ultrasonics GmbH; model UP200s) with a Ø7mm titanium sonotrode following Laumer et al. (2009) [50]. The homogenization is evaluated visually and repeated until a white homogenous 'cloud' of cellulose is attained. The sample is then frozen at -16 °C for at least 12 hours, followed by freeze-drying at -58 °C for 24 hours. The lyophilized samples are stored in tightly closed screw cap polypropylene microtubes, in a desiccator cabinet filled with a silicagel drying agent until isotopic and AMS analysis.

For a typical batch for stable isotopic studies, Ca. 10% of samples per batch are typically selected for determination of cellulose yield, i.e. the mass of obtained α-cellulose versus the mass of wood slivers weighed into cellulose extraction, to monitor the condition of the wood material (c.f. Savard et al. (2012) [47]) and the consistency of the extraction. Depending on material preservation, yields commonly vary between ca. 15 to 50%, with a long-term (5 years; 2016-2020) mean at 34.7% (± 4.8; n=232). Some steps of the cellulose extraction process are shown in Fig. 2.

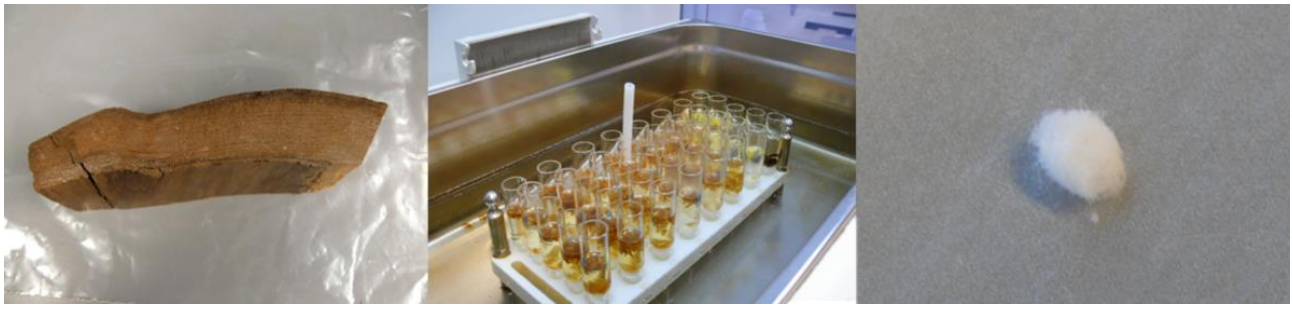

Figure 2. The process flow of the cellulose extraction. Left: The *Larix* sample 30/KAM/79 (dims. L: 110mm, W: 25mm, D: 25mm) . Middle: 40-slot PTFE block of the cellulose extraction system in action with the 30/KAM/79 samples. Right: Resulted α-cellulose sample from the 30/KAM/79 wood (diam. 8mm).

If relevant, stable carbon isotopic composition of the α-cellulose is measured using an NC2500 elemental analyzer (Carlo Erba, Milan, Italy) coupled to a Delta V Plus/Advantage (Thermo Fisher Scientific, Bremen, Germany) isotope ratio mass spectrometer. Depending on the applied helium dilution settings, 70-150 ug of α-cellulose is weighed into 3*4 mm sized tin capsules and tightly folded. The samples are combusted at 1020 °C with automated O_2 injection, followed by chromatographic separation of gases and introduction into the mass spectrometer via the ConFlo IV interface (Thermo Fisher Scientific, Bremen, Germany). The measured $\delta^{13}C$ values (against VPDB) are normalized using the internationally distributed reference materials IAEA-CH6 (-10.45 ‰), IAEA-CH3 (-24.72 ‰) and IAEA-CH7 (-32.15 ‰). Reproducibility is checked with systematic measurements of sample replicates (n=2 to 10). Long-term accuracy and precision are monitored with two in-house quality reference materials (caffeine, cellulose). Both sample repeats and quality checks indicate a reproducibility of ≤ ±0.15‰.

2.3 Combustion and Graphitization

Two different sample treatment methods are used for combusting and converting the combusted CO_2 to graphite targets for ^{14}C-AMS measurements (see also Kasso et al. 2021 [51]). The traditional method, referred to as Closed-Tube-Combustion (CTC), follows primarily the method B of ASTM D6866-20 standard (ASTM 2020) and is utilized, for instance, in Uusitalo et al. (2018) [18]. Chemically pretreated sample is placed inside a pre-cleaned quartz tube sealed from the other end with stoichiometric excess of copper oxide grains. The tube is evacuated to <0.1 mbar pressure and torch-sealed. The sealed ampoule is placed in an oven for combustion in 900°C for at least four hours. The formed CO_2 is collected and cryogenically purified with liquid-N_2 and cold (ca. -85°C) ethanol traps. The CO_2 sample is then converted to graphite with Zn and Fe catalysts as described by Slota et al. (1987) [52] and pressed to an AMS target.

The second method, referred to as EA-HASE, includes Elemental Analyzer (EA) combustion coupled with a LabVIEW controlled CO_2 purification and graphitization line. First, the pretreated sample is placed in a tin cup (Elemental Microanalysis D1001) and combusted in EA (Thermo Scientific Flash 2000 NC, Thermo Fisher Scientific Inc., Waltham, MA, USA). While the temperature of the combustion process (1020°C) is sufficient to oxidize carbon to CO_2, the tin cups used react with oxygen in an exothermic process rising the temperature briefly to 1800°C. Second, the formed CO_2 is cryogenically trapped and purified, and graphitized within the Helsinki Adaptive Sample PrEparation (HASE) line using zinc and iron catalysts [53]. Presently, essentially all the samples are treated with the EA-HASE process after a transition period from CTC to EA-HASE. A schematic view of the system is shown in Fig. 3.

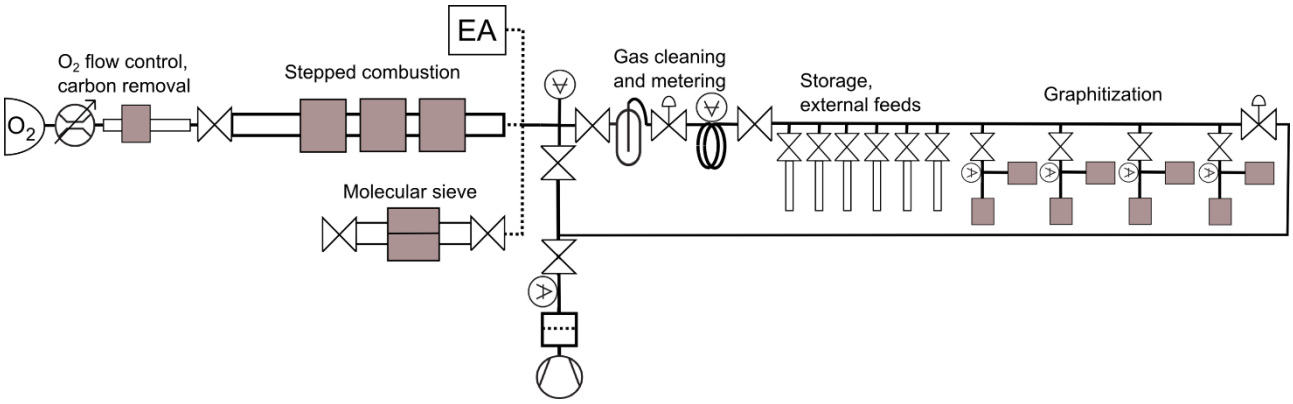

Figure 3. Schematic view of the EA-HASE combustion and graphitization system at the Laboratory of Chronology, Finnish Museum of Natural History, Luomus, University of Helsinki. Adopted from Palonen et al. (2013) [53].

2.4 AMS measurements and data processing

The obtained graphite + Fe samples are pressed into AMS cathodes (2JD032750 Cathode Blank, National Electrostatics Corp., Middleton, WI, USA) by using a pneumatic sample press (PSP, Ionplus AG, Dietikon, Switzerland), mounted on the target wheel and delivered to the ^{14}C analysis in the Helsinki AMS (HAMS). HAMS is based on EGP-10-II 5MV tandem accelerator with two 40-cathode MCGSNICS ion sources from National Electrostatic Corp and has been in operation from 2004 [54]. Since early years of the operation, control electronics of the accelerator have been changed from original in-house built control system to Allen-Bradley factory automation system by Rockwell Automation and fast switching between isotopic masses has been implemented. These have improved the AMS performance drastically [55].

The fast sequential injection of the isotopes, measurements of stable-isotope currents, and processing of rare-isotope events are performed with real-time NI-PXI computers from National Instruments (NI). Injection size parameters are typically re-optimised 1-2 times during long measurements to ensure optimal throughput of the system. Most of the parameters in the accelerator system are controlled with NI network shared variables and stored to the NI Citadel database in real time. As almost all parameters from the accelerator automation system are stored to the same database, AMS data retrieval consists of querying the database upon each cathode measurement of certain time intervals. All of the signal timings, ion energies and electric and magnetic fields can be controlled precisely by changing corresponding network shared variables of the system, which allows reconfiguration of the system easily to different kinds of measurements.

A mean-based method for AMS data-analysis is used for monitoring the quality of the data during the measurements. After the measurements have been completed, the raw data is pulled out from the database and $^{14}C/^{13}C$ and $^{13}C/^{12}C$ ratios for each measurement is derived. Ratios together with measurement time stamp are analyzed using the Bayesian CAR model for AMS data analysis [56]. Bayesian CAR code uses this data to, in addition to the counting uncertainty, infer the changes in the modern standard level reflecting the machine error of a measurement day. Since machine characteristics are intrinsically taken into account, the Bayesian CAR model analysis provides more realistic uncertainties compared to a typical mean-based method [56].

Each measurement batch contains 40 samples of standards, references and unknowns. Oxalic acid II samples (typically 5 pcs, NIST SRM 4990C) are used as a standard material. A pressed ^{14}C-dead natural graphite (14734 Graphite powder, -200 mesh, 99.9999%, Alfa Aesar, Karlsruhe, Germany) target is used to monitor AMS machine characteristics. Additionally, a large-mass blank (lmb) background [57] is monitored with a target of either combusted and graphitized natural graphite (as above) or combusted and graphitized fossil diesel (EN590, Neste Oy, Porvoo, Finland) sample for CTC (N = 13 since 3/2017) and EA-HASE (N = 24, since 3/2017), respectively. Furthermore, when measuring wood cellulose series, we add pretreated, combusted and graphitized cellulose sample of 30/KAM/79 to monitor the full process background. Eventually, the background correction follows an equation:

$$F = F_{uncorr} \cdot (1 + f_{lmb}) - f_{lmb}, \quad (1)$$

in which f_{lmb} = lmb background correction, F_{uncorr} = uncorrected fraction modern of a sample and F = fraction modern of a sample corrected for lmb background. ^{14}C background level (f_{lmb}) is calculated from background sample data of a current sample set and earlier measured sets. Weights of the earlier backgrounds in background calculation decrease exponentially by factor 2/3. Formally, the weight of the n:th set can be calculated through equation $p_n = w(1-w)^n$, where w is the weight factor (currently 2/3) and n = 0 is the current set, n = 1 is the previous etc.. Therefore, for example, $p0 \approx 0.67$ and $p1 \approx 0.22$. Hence, the adopted background is a compromise between long-term average and batch-specific background to a) better take into account the contemporary characteristics of the AMS facility and b) reduce contribution of anomalous, although rare, background measurements.

For routine analyses, precision of ^{14}C-AMS measurement is 0.3%, as defined by half-width of the 68.2% central posterior density interval, corresponding to the standard deviation of the assumed Gaussian distribution of the mean-based method. By extending the measurement time 0.2% precision can be reached. For more detailed account on measurement time and other machine characteristics, see Palonen & Tikkanen (2015)[55].

3. Results and Discussion

3.1 Large-mass blank background values

Measurements of various ^{14}C-dead materials over the recent years allow us to decipher ^{14}C-background components of different processes contributing in the ^{14}C measurements (Table 1). The machine background of HAMS facility has been determined using diamond samples [58] and proven to be extremely low corresponding to radiocarbon ages of ca. 80 000 BP [59]. Additionally, we use high-purity natural graphite (14734 Graphite powder, -200 mesh, 99.9999%, Alfa Aesar, Karlsruhe, Germany) to assess ^{14}C background. Pressed targets of natural graphite (natGr) provide an estimate on combined background contribution of natGR samples, target pressing and AMS measurement of $f_{natGR\text{-}press\text{-}AMS} = 0.0020(9)$. As the machine background is low, this converts to an individual background contribution resulting from the natGr itself and/or from AMS target pressing process: $f_{natGr\text{-}press} = 0.0019(9)$.

The average large-mass blank (lmb) backgrounds measured with combusted and graphitized natGr (>1 mgC) or fossil diesel (>0.5 mgC) samples for CTC and EA-HASE are $f_{lmb,CTC} = 0.0040(15)$ and $f_{lmb,EA\text{-}HASE} = 0.0026(10)$, respectively. Fossil diesel was initially chosen for EA-HASE due to industrial applications and since it has excellent combustion characteristics. The CTC process closely follows a traditional labour-intensive ^{14}C sample preparation process based on combustion of samples in evacuated and close quartz tubes that is used worldwide by ^{14}C laboratories and eventually standardized for biofraction measurements (ASTM, 2020). The obtained background level for this process equals to that of a classical paper of Donahue et al. (1990) [57], i.e. f = 0.004(1).

Table 1. Compilation of ^{14}C background measurements performed at the University of Helsinki.

Process				CTC			EA-HASE			ref.
	N	f_{mean}	σ	N	f_{mean}	σ	N	f_{mean}	σ	
AMS, diamond samples		<0.00005								[59]
natGr – Press – AMS	34	0.0020	0.0009							This study
Combustion – Graphitization – Press – AMS*				13	0.0040	0.0015	24	0.0026	0.0010	This study
Cellulose extraction – Combustion – Graphitization – Press – AMS							7	0.0036	0.0005	This study
natGr – Press		0.0019	0.0009							This study
Combustion, Graphitization					0.0020	0.0019				This study
Cellulose extraction	7	0.0010	0.0011							This study

*This corresponds to the large-mass blank background f_{lmb}. For individual sample batches, the large-mass blank background is evaluated as weighted average as described in the methods. Thus the values may slightly differ from batch to batch.

The difference between pressed and combusted – graphitized – pressed targets made of natGr allows for estimating background contribution from combustion and graphitization processes for CTC: $f_{comb\text{-}graph,CTC}$ = 0.0020(19). Concerning CTC the long-term lmb background ($f_{lmb,CTC}$ = 0.0040(15)) is thus equally due to natGr sample & target pressing ($f_{natGR\text{-}press}$ = 0.0019(9)) and from combustion & graphitization ($f_{comb\text{-}graph,CTC}$ = 0.0020(19)). It seems that the long-term lmb background if smaller for EA-HASE process: $f_{lmb,EA\text{-}HASE}$ = 0.0026(10). The difference between CTC and EA-HASE may involve contributions from different materials (natGr vs. fossil diesel) used for estimating f_{lmb} and from the EA-HASE process being automatized and optimized for smaller samples thus assumably yielding to smaller background.

Comparison of the results of the ^{14}C-dead cellulose measurements ($f_{cell,EA\text{-}HASE}$ = 0.0036(5)) and lmb measurement made with EA-HASE allow for estimating the background contribution from the cellulose extraction to be f_{cell} = 0.0010(11). Essentially, the data is reasonable as the lowest ^{14}C level is observed for the pressed graphite targets, slightly larger for combustion – graphitization – press – AMS process and again equally larger for the whole cellulose measurement process.

3.2 Mass dependencies

To compare the CTC and EA-HASE processes to produce wood-based AMS graphite targets, test sets as a function of AMS graphite mass were produced. The ^{14}C-dead wood (*Larix*, 30/KAM/79) samples [37] were pretreated to cellulose, divided to subsamples of certain masses, combusted and graphitized through CTC (so far 5 pcs) and EA-HASE (so far 11 pcs) processes and measured with the Helsinki AMS (see Methods).

The results for both CTC and EA-HASE processes with varying sample masses are shown in Fig. 4 and Table 2, respectively. Both curves show consistent mass-dependency with smaller samples having higher F values, as expected. The EA-HASE curve is consistently on a lower level and it more rapidly converges to a smaller F value. As the cellulose pre-treatment protocol is identical for both lines, it means that the EA-HASE process introduces less ^{14}C contamination to the samples compared to CTC. This is in line with the observation of larger lmb background in case of CTC. Particularly, larger volumes applied for combustion and purification within the CTC process seem to act as more effective storage of carbon possibly resulting in also larger mass-dependent background component.

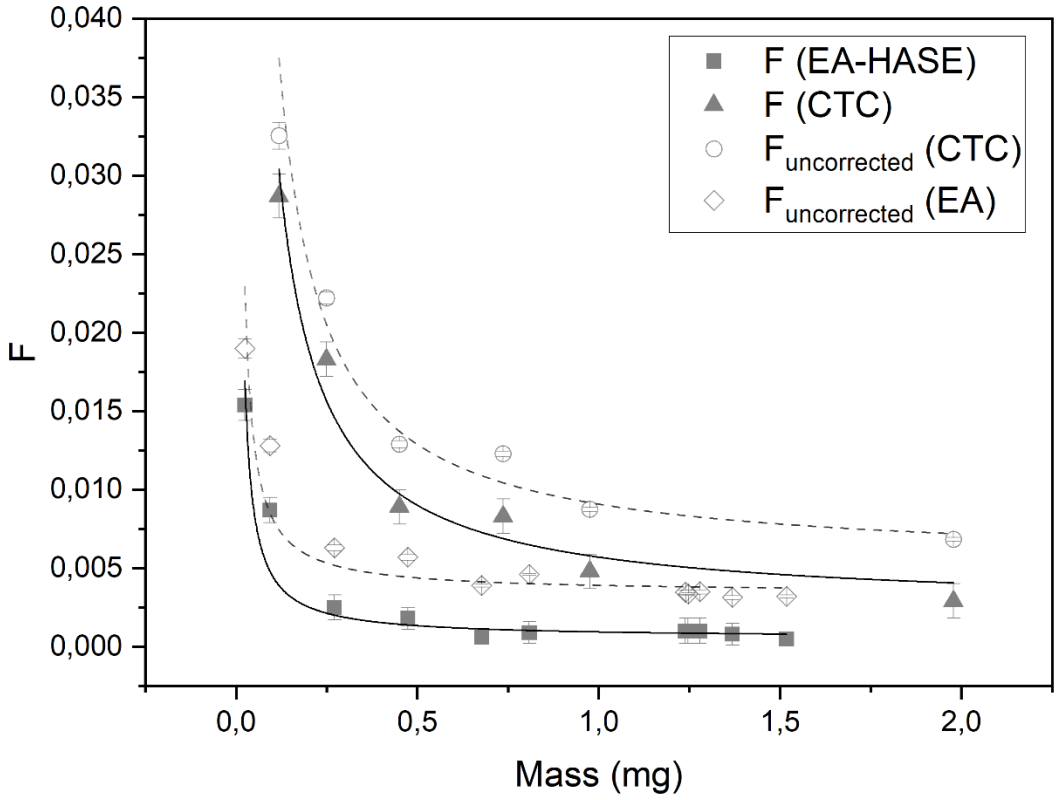

Figure 4. Mass-balance measurements using both the EA-HASE and CTC lines. Dark grey symbols show the large-mass blank corrected values for both lines whereas transparent symbols show the uncorrected ones. Solid and dashed lines show the respective best fits for the data. The x-axis shows the carbon mass of the sample. The dashed lines approach the long-term background of the respective lines with EA-HASE plateauing more quickly as sample mass increases. These measurements are not fully representative of the long-term average background (f_{lmb}, Table 1) due to the procedure to define the background (see Methods).

According to Roberts et al. (2019) [60], the mass-dependency can be understood through the following equation:

$$F = (F_{unknown} * m_{unknown} + F_{cont} * m_{cont})/(m_{unknown} + m_{cont}) \quad (2)$$

where F is the measured large-mass blank corrected ^{14}C content, $F_{unknown}$ is the unknown or true ^{14}C content, $m_{unknown}$ is the unknown or true sample mass, F_{cont} is the assumed ^{14}C content of the contaminant, m_{cont} is the mass of the contaminant and $m = m_{unknown} + m_{cont}$ is the full sample mass. From the equation it follows that as m_{cont} approaches zero, the equation approximates to $F = F_{unknown} * m / m = F_{unknown}$. Similarly, when m_{cont} approaches m, the equation approximates to $F = F_{cont} * m / m = F_{cont}$. Assuming the contaminant mass stays constant, decreasing sample mass increases the contamination effect in a non-linear way, as is observed in Fig. 4.

3.3 Mass-balance blank correction

This contamination is referred to as mass-balance blank (mbb) background. Based on Eq. 1, increasing the sample mass should lead to F approaching zero. In practice this is not the case as the measurement process introduces contamination that scales in proportional to the mass. Further, one can advance to mass-balance blank correction i.e. to correct for the effect due to small sample mass. Various methods have been developed for determining the F_{cont} [21,22,61], but those applications mainly concern with microscale compound-specific measurements where the contamination sources are more varied. With respect to tree-ring analyses, the contamination primarily comes from the vacuum line and combustion processes where the contaminant is presumably mostly modern carbon, so the F_{cont} should be close to 1. Thus, by assuming a constant F_{cont}, m_{cont} can be determined by fitting a function of Eq. 2 to the measurements, as seen in Fig. 4. The values for the fitted parameters and their 1σ uncertainties are in Table 2.

Table 2. Determined parameter values and their 1σ uncertainties for EA-HASE and CTC processes.

	EA-HASE	**σ**	**CTC**	**σ**
F_{cont}	1	N/A	1	N/A
m_{cont} (mgC)	0.00040	0.00004	0.0033	0.00033

The mass of the contaminant within the EA-HASE process is an order of magnitude smaller than the corresponding CTC value: $m_{cont,\ EA\text{-}HASE}$ = 0.00040 mgC vs. $m_{cont,\ CTC}$ = 0.0033 mgC. Although not strictly equivalent, as we have assumed a fixed F_{cont} representing modern carbon, our values are comparable to those of obtained by e.g. NOSAMS (m_{cont} = 0.0021 mgC) [60] the EA-HASE process being even better.

Eventually, $F_{unknown}$ can be solved from Eq. 2 to give the mass-corrected or true F of the sample

$$F_{unknown} = (F * m_{meas} – F_{cont} * m_{cont})/(m_{meas} – m_{cont}) \quad (3)$$

in which F is the large-mass blank i.e. background corrected value.

It should be noted that this approach gains from a larger data set of mass-dependent measurements that we pursue in more detail in the future to be able to also assess time and sample-type dependency of the mbb correction.

3.4 Age-dependency of mass-balance blank correction

Adopting the EA-HASE parameter values from Table 2, it is possible to perform mass-balance corrections with given F and m_{meas} using Eq. 3. For our analysis, we have defined three distinct time periods that are currently considered being of worldwide interest and also to our consortium: 1) ^{14}C ages that cover the Common Era (1950 – 0 BP), including the Miyake event of AD 774/775, 2) ^{14}C ages that overlap the Minoan eruption of Thera/Santorini (4 – 3 kyr BP), and 3) ^{14}C ages close to the ^{14}C measurement limit, including the Laschamp event (48 – 35 kyr BP). The contour visualization assuming these periods and sample masses ranging from 0.2 to 1.5 mgC can be seen in Fig 5.

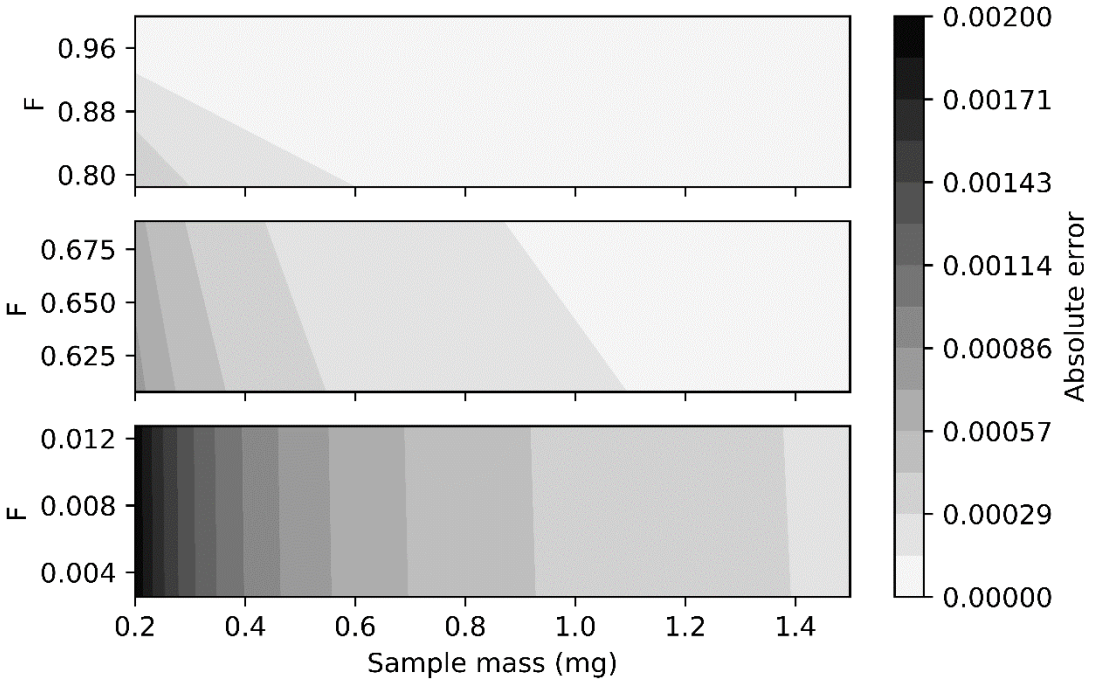

Figure 5. Contour plot showing the mass-balance effects for ^{14}C ages 1950 – 0 BP (upper), 4000 – 3000 BP (middle) and 48000 – 35000 BP (lower). Absolute error is the difference between measured and true ^{14}C of the sample, i.e. $F - F_{unknown}$. The x-axis shows the carbon mass of the sample.

For the Common era (1, Fig. 5, upper), the mass-balance effect is insignificant. Even a small sample with a mass of 0.2 mgC results in an absolute systematic increase of F by only 0.0004 – ~0, which is an order of magnitude less than the typical statistical uncertainty of ca. δF = 0.003 for these ages. As can be seen from Fig. 5, the mass-balance effect for this period tends towards zero with masses above 0.6 mgC, regardless of age. Considering the Minoan era (2, Fig. 5, middle), the effect is still small: a sample mass of 0.2 mgC would result in an absolute systematic increase of F by 0.0008 – 0.0006. The effect can be translated into a shift of 0.13 - 0.09% in age, with older ^{14}C ages exhibiting slightly higher relative errors. As a practical example, measuring the same sample material, but with masses of 0.5 mgC and 1.0 mgC, around the assumed Santorini eruption date of approximately 3550 cal BP the difference would translate into a ^{14}C age difference of 1.8 years. Similarly, applying the analysis for the time period of the Miyake event (AD 770), the mass difference would translate into a ^{14}C difference of 0.5 ^{14}C years. To put these numbers into perspective, our typical ^{14}C age error for both periods is approximately 15-30 ^{14}C years. In both cases, the effect is insignificant.

Going further back in time towards the ^{14}C limit (3, Fig. 5, lower), the mass-balance effects start to become more noticeable for ^{14}C ages. Laboratories are typically using 1 mg carbon target masses as safe estimates for sample sizes. However, even such mass would result in a systematic increase of F by approximately 0.0004. At 48000 BP this would translate into an age shift of about 1350 ^{14}C years, whereas at 35000 BP the shift would be approximately 250 ^{14}C years. The markedly larger shift in the upper limit is caused by the logarithmic nature of the age conversion as uncertainties near the ^{14}C background are amplified and asymmetric in age. Recently, Laschamp event of 42 kyr BP was studied through ^{14}C measurements from New Zealand swamp kauri tree-rings by liquid scintillation method [62] free from mass-balance effects. These measurements in radiocarbon age range from approximately 42k to 36k BP and the measurement

uncertainty ranges typically from ~120 to ~250 ^{14}C years. These uncertainties are of similar magnitude than the mass-balance effects we observe for our ^{14}C-AMS process with 1 mgC samples around the same age range. Mass-balance effects need to be considered particularly for repeated measurements of different sample masses. As an example, measuring the same 35k BP year old sample twice but with masses of 1 mgC and 2 mgC results in an age difference of approximately 130 ^{14}C years. For ^{14}C time-series measurements, retaining the precise chronological order and shape are often crucial. Therefore, in addition to recognizing the potential systematic biases (i.e. baseline shifts), it is important to understand the more random mass-related effects that might arise from varying sample sizes.

As a summary, we can conclude that the mass-balance effects observed within our ^{14}C measurement process for wood cellulose are insignificant for periods 1) and 2) but need to be considered for period 3) closer to ^{14}C background levels. Fortunately, for mass-balance effects, the minimization routine is straightforward. Considering e.g. the Laschamp example, increasing sample masses to over 2 mgC would reduce the ^{14}C age bias to less than 100 years, which is less than the typical error. More importantly, keeping sample masses between 2 mgC – 2.5 mgC reduces the mass-balance induced sample-to-sample error to less than 25 years. Moreover, correction for systematic mass-balance effects can be performed based on the available data that continues to be upgraded.

The above analysis is based on the corrections parameters found for the EA-HASE process. It is relevant to assess the effects also for the CTC process, as it was recently used for annual and earlywood-latewood measurements [18] of the Miyake event. By performing the mass-balance correction for those measurements, we find that the average effect for the decay-corrected Δ^{14}C is 0.3‰, which is an order of magnitude less than the typical measurement error. Furthermore, the effect is mainly systematic, meaning that it affects all samples nearly equally. Therefore, we conclude the effect being insignificant concerning the data presented in Uusitalo et al (2018) [18].

4. Conclusions

In this paper, we have presented a recipe to obtain reliable tree-ring samples for ^{14}C content measurements from the high-latitude trees by a consortium between the University of Helsinki and Natural Resources Institute Finland. This includes describing the dendrochronology, pretreatment procedures, background corrections, uncertainty calculations and data processing, all being part of the International Calibration (IntCal) criteria [63,64]. Particularly, we have shown that both the traditional Closed-Tube-Combustion and the more advanced Elemental Analyzer –based process yield to high-quality data, the latter being more optimized for small and close-to-background samples. Furthermore, we have performed a test measurement set for inferring the mass-balance effects for tree-ring measurements. Based on these measurements we have constructed a correction curve and studied the mass-balance effects for samples ranging from the Common Era towards the Pleistocene i.e. the ^{14}C measurement limit. The main finding of these analyses has been that the mass-balance effects are insignificant for ages up to several millennia, including the Santorini eruption period (4 – 3 kyr BP), but start to become more important when approaching the ^{14}C limit, especially for high-precision applications. The effective solution is to increase and unify sample masses, which reduces both systematic and random mass-balance related errors. Furthermore, an alpha-cellulose control sample of ^{14}C-dead wood prepared with the same pretreatment procedure with a size comparable to the actual samples helps to track and assure the quality of the whole procedure and gradually expands the data set for the correction curve.

Presently, the data allows preliminary mass-balance corrections, particularly for very old samples and for young samples to rule corrections out. In the future, as the data set extends, the fit parameters are

automatically adjusted to additional data within Python programming environment we have adopted to support our quality control. The fit parameters are included within Laboratory Information Management System (LIMS) to enable automated informing in case of suspected mass-balance effects.

So far, this development has resulted in the first observation of the potential latitudinal differences of the intensities of the solar ^{14}C excursions [18] as well as in the collaboration to study the ^{14}C increase of AD 1054/1055 [8]. The work paves the way for both our procedures and high-latitude tree-ring archives of Finland to gain more visibility in the international research environment.

Acknowledgements: The authors wish to thank Tauno Luosujärvi for his significant contributions to laboratory work in the tree-ring projects of this consortium, GTK and Raimo Sutinen for providing the 30/KAM/79 sample, and Hanna Turunen, Anne-Maija Forss, Kari Eskola and Igor Shevchuk for sample pretreatment and isotope work, and Pietari Kienanen for AMS analyses.

Funding: The work has been supported by grants from the Academy of Finland (251287, 251441, 288083, 288267) and by the Magnus Ehrnrooth foundation and The Finnish Cultural Foundation.

Competing interests: The authors declare no competing interests.

References:

[1] F. Miyake, K. Nagaya, K. Masuda, T. Nakamura, A signature of cosmic-ray increase in AD 774–775 from tree rings in Japan, Nature. 486 (2012) 240–242. https://doi.org/10.1038/nature11123.

[2] F. Miyake, K. Masuda, T. Nakamura, Another rapid event in the carbon-14 content of tree rings., Nat. Commun. 4 (2013) 1748. https://doi.org/10.1038/ncomms2783.

[3] J. Park, J. Southon, S. Fahrni, P.P. Creasman, R. Mewaldt, Relationship between solar activity and Δ14C peaks in AD 775, AD 994, and 660 BC, Radiocarbon. 59 (2017) 1147–1156. https://doi.org/10.1017/RDC.2017.59.

[4] A. Fogtmann-Schulz, S.M. Østbø, S.G.B. Nielsen, J. Olsen, C. Karoff, M.F. Knudsen, Cosmic ray event in 994 C.E. recorded in radiocarbon from Danish oak, Geophys. Res. Lett. 44 (2017) 8621–8628. https://doi.org/10.1002/2017GL074208.

[5] A.Z. Rakowski, M. Kraępiec, M. Huels, J. Pawlyta, M. Boudin, Increase in radiocarbon concentration in tree rings from kujawy village (Se Poland) Around Ad 993-994, in: Radiocarbon, Cambridge University Press, 2018: pp. 1249–1258. https://doi.org/10.1017/RDC.2018.74.

[6] F. Miyake, A.J.T. Jull, I.P. Panyushkina, L. Wacker, M. Salzer, C.H. Baisan, T. Lange, R. Cruz, K. Masuda, T. Nakamura, Large 14C excursion in 5480 BC indicates an abnormal sun in the mid-Holocene., Proc. Natl. Acad. Sci. U. S. A. 114 (2017) 881–884. https://doi.org/10.1073/pnas.1613144114.

[7] A.J.T. Jull, I. Panyushkina, F. Miyake, K. Masuda, T. Nakamura, T. Mitsutani, T.E. Lange, R.J. Cruz, C. Baisan, R. Janovics, T. Varga, M. Molnár, More rapid 14C excursions in the tree-ring record: A record of different kind of solar activity at about 800 BC?, in: Radiocarbon, Cambridge University Press, 2018: pp. 1237–1248. https://doi.org/10.1017/RDC.2018.53.

[8] F. Terrasi, F. Marzaioli, R. Buompane, I. Passariello, G. Porzio, M. Capano, S. Helama, M. Oinonen, P. Nöjd, J. Uusitalo, A.J.T. Jull, I.P. Panyushkina, C. Baisan, M. Molnar, T. Varga, G. Kovaltsov, S. Poluianov, I. Usoskin, CAN THE 14 C PRODUCTION IN 1055 CE BE AFFECTED BY SN1054? ,

Radiocarbon. 00 (2020) 1–16. https://doi.org/10.1017/rdc.2020.58.

[9] C. Oppenheimer, L. Wacker, J. Xu, J.D. Galván, M. Stoffel, S. Guillet, C. Corona, M. Sigl, N. Di Cosmo, I. Hajdas, B. Pan, R. Breuker, L. Schneider, J. Esper, J. Fei, J.O.S. Hammond, U. Büntgen, Multi-proxy dating the 'Millennium Eruption' of Changbaishan to late 946 CE, Quat. Sci. Rev. 158 (2017) 164–171. https://doi.org/10.1016/j.quascirev.2016.12.024.

[10] M. Hakozaki, F. Miyake, T. Nakamura, K. Kimura, K. Masuda, M. Okuno, Verification of the Annual Dating of the 10th Century Baitoushan Volcano Eruption Based on an AD 774–775 Radiocarbon Spike, Radiocarbon. (2017) 1–8. https://doi.org/10.1017/RDC.2017.75.

[11] M.W. Dee, B.J.S. Pope, Anchoring historical sequences using a new source of astro-chronological tie-points, Proc. R. Soc. A Math. Phys. Eng. Sci. 472 (2016). https://doi.org/10.1098/rspa.2016.0263.

[12] U. Büntgen, V.S. Myglan, F.C. Ljungqvist, M. McCormick, N. Di Cosmo, M. Sigl, J. Jungclaus, S. Wagner, P.J. Krusic, J. Esper, J.O. Kaplan, M.A.C. de Vaan, J. Luterbacher, L. Wacker, W. Tegel, A. V. Kirdyanov, Cooling and societal change during the Late Antique Little Ice Age from 536 to around 660 AD, Nat. Geosci. 9 (2016) 231–236. https://doi.org/10.1038/ngeo2652.

[13] C.L. Pearson, P.W. Brewer, D. Brown, T.J. Heaton, G.W.L. Hodgins, A.J. Timothy Jull, T. Lange, M.W. Salzer, Annual radiocarbon record indicates 16th century BCE date for the Thera eruption, Sci. Adv. 4 (2018) eaar8241. https://doi.org/10.1126/sciadv.aar8241.

[14] R. Friedrich, B. Kromer, L. Wacker, J. Olsen, S. Remmele, S. Lindauer, A. Land, C. Pearson, A NEW ANNUAL 14 C DATASET FOR CALIBRATING THE THERA ERUPTION , Radiocarbon. 62 (2020) 1–9. https://doi.org/10.1017/rdc.2020.33.

[15] M. Kuitems, J. van der Plicht, E. Jansma, WOOD FROM THE NETHERLANDS AROUND THE TIME OF THE SANTORINI ERUPTION DATED BY DENDROCHRONOLOGY AND RADIOCARBON, Radiocarbon. 62 (2020) 1–5. https://doi.org/10.1017/rdc.2020.23.

[16] C. Pearson, L. Wacker, A. Bayliss, D. Brown, M. Salzer, P. Brewer, S. Bollhalder, G. Boswijk, G. Hodgins, ANNUAL VARIATION IN ATMOSPHERIC 14 C BETWEEN 1700 BC AND 1480 BC , Radiocarbon. 62 (2020) 1–14. https://doi.org/10.1017/rdc.2020.14.

[17] M. Stuiver, T.F. Braziunas, Anthropogenic and solar components of hemispheric 14C, Geophys. Res. Lett. 25 (1998) 329–332. https://doi.org/10.1029/97GL03694.

[18] J. Uusitalo, L. Arppe, T. Hackman, S. Helama, G. Kovaltsov, K. Mielikäinen, H. Mäkinen, P. Nöjd, V. Palonen, I. Usoskin, M. Oinonen, Solar superstorm of AD 774 recorded subannually by Arctic tree rings, Nat. Commun. 9 (2018) 3495. https://doi.org/10.1038/s41467-018-05883-1.

[19] U. Büntgen, L. Wacker, J.D. Galván, S. Arnold, D. Arseneault, M. Baillie, J. Beer, M. Bernabei, N. Bleicher, G. Boswijk, A. Bräuning, M. Carrer, F.C. Ljungqvist, P. Cherubini, M. Christl, D.A. Christie, P.W. Clark, E.R. Cook, R. D'Arrigo, N. Davi, Ó. Eggertsson, J. Esper, A.M. Fowler, Z. Gedalof, F. Gennaretti, J. Grießinger, H. Grissino-Mayer, H. Grudd, B.E. Gunnarson, R. Hantemirov, F. Herzig, A. Hessl, K.-U. Heussner, A.J.T. Jull, V. Kukarskih, A. Kirdyanov, T. Kolář, P.J. Krusic, T. Kyncl, A. Lara, C. LeQuesne, H.W. Linderholm, N.J. Loader, B. Luckman, F. Miyake, V.S. Myglan, K. Nicolussi, C. Oppenheimer, J. Palmer, I. Panyushkina, N. Pederson, M. Rybníček, F.H. Schweingruber, A. Seim, M. Sigl, O. Churakova, J.H. Speer, H.-A. Synal, W. Tegel, K. Treydte, R. Villalba, G. Wiles, R. Wilson, L.J. Winship, J. Wunder, B. Yang, G.H.F. Young, Tree rings reveal globally coherent signature of cosmogenic radiocarbon events in 774 and 993 CE, Nat. Commun. 9 (2018) 3605. https://doi.org/10.1038/s41467-018-06036-0.

[20] D.J. Donahue, T.W. Linick, A.J.T. Jull, Isotope-ratio and background corrections for accelerator mass spectrometry radiocarbon measurements, Radiocarbon. 32 (1990) 135–142.

https://doi.org/10.1017/S0033822200040121.

[21] T.A. Brown, J.R. Southon, Corrections for contamination background in AMS 14C measurements, Nucl. Instruments Methods Phys. Res. Sect. B Beam Interact. with Mater. Atoms. 123 (1997) 208–213. https://doi.org/10.1016/S0168-583X(96)00676-3.

[22] J. Hwang, E.R.M. Druffel, Blank correction for Δ14C measurements in organic compound classes of oceanic particulate matter, Radiocarbon. 47 (2005) 75–87. https://doi.org/10.1017/s0033822200052218.

[23] F.H. Schweingruber, Tree Rings; Basics and Applications of Dendrochronology, 1988.

[24] J.H. Speer, Fundamentals of Tree-ring Research, The University of Arizona Press, Tucson, 2010.

[25] M. Lindholm, Reconstruction of past climate from ring-width chronologies of Scots pine (Pinus sylvestris L.) at the northern forest limit in Fennoscandia, University of Joensuu, 1996.

[26] H.M. Henttonen, P. Nöjd, S. Suvanto, J. Heikkinen, H. Mäkinen, Large trees have increased greatly in Finland during 1921–2013, but recent observations on old trees tell a different story, Ecol. Indic. (2019). https://doi.org/10.1016/j.ecolind.2018.12.015.

[27] L. Kullman, O. Engelmark, A high Late Holocene tree-limit and the establishment of the spruce forest-limit – a case study in northern Sweden, Boreas. (1990). https://doi.org/10.1111/j.1502-3885.1990.tb00136.x.

[28] S. Helama, M. Kuoppamaa, R. Sutinen, Subaerially preserved remains of pine stemwood as indicators of late Holocene timberline fluctuations in Fennoscandia, with comparisons of tree-ring and 14C dated depositional histories of subfossil trees from dry and wet sites, Rev. Palaeobot. Palynol. 278 (2020) 104223. https://doi.org/10.1016/j.revpalbo.2020.104223.

[29] M. Eronen, The retreat of pine forest in Finnish Lapland since the Holocene climatic optimum: a general discussion with radiocarbon evidence from subfossil pines., Fennia. (1979).

[30] M. Eronen, P. Zetterberg, K.R. Briffa, M. Lindholm, J. Meriläinen, M. Timonen, The supra-long Scots pine tree-ring record for Finnish Lapland: Part 1, chronology construction and initial inferences, The Holocene. 12 (2002) 673–680. https://doi.org/10.1191/0959683602hl580rp.

[31] M. Lindholm, J. Merilainen, M. Eronen, A 1,250-year ring-width chronology of Scots pine for South-eastern Finland, in the southern part of the boreal forest belt, Dendrochronologia. (1998).

[32] S. Helama, M. Lindholm, J. Meriläinen, M. Timonen, M. Eronen, Multicentennial ring-width chronologies of Scots pine along a north-south gradient across Finland, Tree-Ring Res. (2005). https://doi.org/10.3959/1536-1098-61.1.21.

[33] S. Helama, J. Holopainen, M. Timonen, K. Mielikainen, An 854-year tree-ring chronology of scots pine for South-West Finland, Stud. Quat. (2014). https://doi.org/10.2478/squa-2014-0006.

[34] S. Helama, T.P. Luoto, L. Nevalainen, J. Edvardsson, Rereading a tree-ring database to illustrate depositional histories of subfossil trees, Palaeontol. Electron. (2017). https://doi.org/10.26879/696.

[35] S. Helama, K. Mielikäinen, M. Timonen, M. Eronen, Finnish supra-long tree-ring chronology extended to 5634 BC, Nor. Geogr. Tidsskr. - Nor. J. Geogr. (2008). http://www.tandfonline.com/doi/abs/10.1080/00291950802517593 (accessed January 25, 2016).

[36] S. Helama, P. Saranpää, C.L. Pearson, L. Arppe, J. Holopainen, H. Mäkinen, K. Mielikäinen, P. Nöjd, R. Sutinen, J.P. Taavitsainen, M. Timonen, J. Uusitalo, M. Oinonen, Frost rings in 1627 BC and AD 536 in subfossil pinewood from Finnish Lapland, Quat. Sci. Rev. 204 (2019) 208–215. https://doi.org/10.1016/j.quascirev.2018.11.031.

[37] K. Mäkinen, Tiedonanto Vuotson interglasiaalisesta lehtikuusen rungosta [Report on interglacial Larix trunk at Vuotso, Northern Finland], Geologi. 1982 (1982) 183–185.

[38] M. Stokes, T. Smiley, An Introduction to Tree-ring Dating, University of Chicago Press, Chicago, 1968.

[39] H.C. Fritts, Tree Rings and Climate, Academic Press, New York, 1976.

[40] R.L. Holmes, Computer-assisted quality control in treering dating and measurement, Tree-Ring Bull. 43 (1983) 69–75.

[41] F. Rinn, Time series analysis and presentation for dendrochronology and related applications, (2006).

[42] M. Rydval, L.Å. Larsson, L. McGlynn, B.E. Gunnarson, N.J. Loader, G.H.F. Young, R. Wilson, Blue intensity for dendroclimatology: Should we have the blues? Experiments from Scotland, Dendrochronologia. (2014). https://doi.org/10.1016/j.dendro.2014.04.003.

[43] C. Bronk Ramsey, J. Van Der Flicht, B. Weninger, “Wiggle matching” radiocarbon dates, Radiocarbon. (2001). https://doi.org/10.1017/s0033822200038248.

[44] M. Galimberti, C.B. Ramsey, S.W. Manning, Wiggle-match dating of tree-ring sequences, Radiocarbon. 46 (2004) 917–924. https://doi.org/10.1017/S0033822200035967.

[45] M. Oinonen, E. Hilasvuori, H. Mehtonen, K. Uotila, P. Zetterberg, On the Eve of Urbanization: Bayesian Model Dating for Medieval Turku, Radiocarbon. 55 (2013) 1265–1277. https://doi.org/10.1017/s0033822200048177.

[46] M.P. Denne, Definition of Latewood According to Mork (1928), IAWA J. 10 (1989) 59–62. https://doi.org/10.1163/22941932-90001112.

[47] M.M. Savard, C. Bégin, J. Marion, D. Arseneault, Y. Bégin, Evaluating the integrity of C and O isotopes in sub-fossil wood from boreal lakes, Palaeogeogr. Palaeoclimatol. Palaeoecol. (2012). https://doi.org/10.1016/j.palaeo.2012.06.003.

[48] T. Wieloch, G. Helle, I. Heinrich, M. Voigt, P. Schyma, A novel device for batch-wise isolation of α-cellulose from small-amount wholewood samples, Dendrochronologia. 29 (2011) 115–117. https://doi.org/10.1016/j.dendro.2010.08.008.

[49] K.T. Rinne, T. Boettger, N.J. Loader, I. Robertson, V.R. Switsur, J.S. Waterhouse, On the purification of α-cellulose from resinous wood for stable isotope (H, C and O) analysis, Chem. Geol. (2005). https://doi.org/10.1016/j.chemgeo.2005.06.010.

[50] W. Laumer, L. Andreu, G. Helle, G.H. Schleser, T. Wieloch, H. Wissel, A novel approach for the homogenization of cellulose to use micro‐amounts for stable isotope analyses, Rapid Commun. Mass Spectrom. 23 (2009) 1934–1940. https://doi.org/10.1002/rcm.4105.

[51] T.M. Kasso, M.J. Oinonen, K. Mizohata, J.K. Tahkokallio, T.M. Heikkilä, Volumes of worth-delimiting the sample size for radiocarbon dating of parchment, Radiocarbon. 63 (2021) 105–120. https://doi.org/10.1017/RDC.2020.128.

[52] P.J. Slota, A.J.T. Jull, T.W. Linick, L.J. Toolin, Preparation of Small Samples for 14 C Accelerator Targets by Catalytic Reduction of CO , Radiocarbon. (1987). https://doi.org/10.1017/s0033822200056988.

[53] V. Palonen, A. Pesonen, T. Herranen, P. Tikkanen, M. Oinonen, HASE - The Helsinki adaptive sample preparation line, Nucl. Instruments Methods Phys. Res. Sect. B Beam Interact. with Mater. Atoms. 294 (2013) 182–184. https://doi.org/10.1016/j.nimb.2012.08.056.

[54] P. Tikkanen, V. Palonen, H. Jungner, J. Keinonen, AMS facility at the University of Helsinki, Nucl.

Instruments Methods Phys. Res. Sect. B Beam Interact. with Mater. Atoms. 223–224 (2004) 35–39. https://doi.org/10.1016/j.nimb.2004.04.011.

[55] V. Palonen, P. Tikkanen, A novel upgrade to Helsinki AMS: Fast switching of isotopes with electrostatic deflectors, Nucl. Instruments Methods Phys. Res. Sect. B Beam Interact. with Mater. Atoms. 361 (2015) 263–266. https://doi.org/10.1016/j.nimb.2015.04.053.

[56] V. Palonen, P. Tikkanen, J. Keinonen, Improving AMS uncertainties and detection of instrumental error, Nucl. Instruments Methods Phys. Res. Sect. B Beam Interact. with Mater. Atoms. 268 (2010) 972–975. https://doi.org/10.1016/j.nimb.2009.10.077.

[57] D.J. Donahue, A.J.T. Jull, L.J. Toolin, Radiocarbon measurements at the University of Arizona AMS facility, Nucl. Inst. Methods Phys. Res. B. 52 (1990) 224–228. https://doi.org/10.1016/0168-583X(90)90410-V.

[58] R.E. Taylor, J. Southon, Use of natural diamonds to monitor 14C AMS instrument backgrounds, Nucl. Instruments Methods Phys. Res. Sect. B Beam Interact. with Mater. Atoms. 259 (2007) 282–287. https://doi.org/10.1016/j.nimb.2007.01.239.

[59] V. Palonen, Accelerator mass spectrometry and Bayesian data analysis, University of Helsinki, 2008.

[60] M.L. Roberts, K.L. Elder, W.J. Jenkins, A.R. Gagnon, L. Xu, J.D. Hlavenka, B.E. Longworth, 14 C Blank Corrections for 25–100 μg Samples at the National Ocean Sciences AMS Laboratory , Radiocarbon. 61 (2019) 1403–1411. https://doi.org/10.1017/rdc.2019.74.

[61] S. Sun, V.D. Meyer, A.M. Dolman, M. Winterfeld, J. Hefter, W. Dummann, C. McIntyre, D.B. Montluçon, N. Haghipour, L. Wacker, T. Gentz, T.S. Van Der Voort, T.I. Eglinton, G. Mollenhauer, 14C Blank Assessment in Small-Scale Compound-Specific Radiocarbon Analysis of Lipid Biomarkers and Lignin Phenols, Radiocarbon. 62 (2020). https://doi.org/10.1017/RDC.2019.108.

[62] A. Cooper, C.S.M. Turney, J. Palmer, A. Hogg, M. McGlone, J. Wilmshurst, A.M. Lorrey, T.J. Heaton, J.M. Russell, K. McCracken, J.G. Anet, E. Rozanov, M. Friedel, I. Suter, T. Peter, R. Muscheler, F. Adolphi, A. Dosseto, J. Tyler Faith, P. Fenwick, C.J. Fogwill, K. Hughen, M. Lipson, J. Liu, N. Nowaczyk, E. Rainsley, C.B. Ramsey, P. Sebastianelli, Y. Souilmi, J. Stevenson, Z. Thomas, R. Tobler, R. Zech, A global environmental crisis 42,000 years ago, Science (80-.). 371 (2021) 811–818. https://doi.org/10.1126/science.abb8677.

[63] P.J. Reimer, E. Bard, A. Bayliss, J.W. Beck, P.G. Blackwell, C.B. Ramsey, D.M. Brown, C.E. Buck, R.L. Edwards, M. Friedrich, P.M. Grootes, T.P. Guilderson, H. Haflidason, I. Hajdas, C. Hatté, T.J. Heaton, A.G. Hogg, K.A. Hughen, K.F. Kaiser, B. Kromer, S.W. Manning, R.W. Reimer, D.A. Richards, E.M. Scott, J.R. Southon, C.S.M. Turney, J. van der Plicht, Selection and Treatment of Data for Radiocarbon Calibration: An Update to the International Calibration (IntCal) Criteria, Radiocarbon. 55 (2013) 1923–1945. https://doi.org/10.2458/azu_js_rc.55.16955.

[64] P.J. Reimer, W.E.N. Austin, E. Bard, A. Bayliss, P.G. Blackwell, C. Bronk Ramsey, M. Butzin, H. Cheng, R.L. Edwards, M. Friedrich, P.M. Grootes, T.P. Guilderson, I. Hajdas, T.J. Heaton, A.G. Hogg, K.A. Hughen, B. Kromer, S.W. Manning, R. Muscheler, J.G. Palmer, C. Pearson, J. Van Der Plicht, R.W. Reimer, D.A. Richards, E.M. Scott, J.R. Southon, C.S.M. Turney, L. Wacker, F. Adolphi, U. Büntgen, M. Capano, S.M. Fahrni, A. Fogtmann-Schulz, R. Friedrich, P. Köhler, S. Kudsk, F. Miyake, J. Olsen, F. Reinig, M. Sakamoto, A. Sookdeo, S. Talamo, The IntCal20 Northern Hemisphere Radiocarbon Age Calibration Curve (0-55 cal kBP), Radiocarbon. 62 (2020) 725–757. https://doi.org/10.1017/RDC.2020.41.